Faraday Discussions

Accepted Manuscript

This manuscript will be presented and discussed at a forthcoming Faraday Discussion meeting. All delegates can contribute to the discussion which will be included in the final volume.

Register now to attend! Full details of all upcoming meetings: http://rsc.li/fd-upcoming-meetings

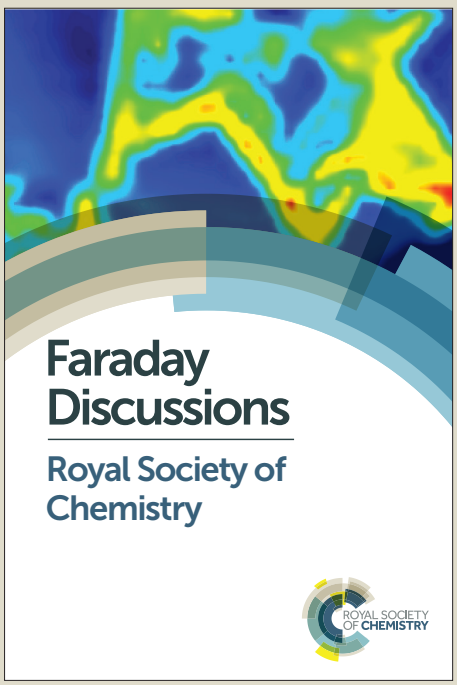

This is an *Accepted Manuscript*, which has been through the Royal Society of Chemistry peer review process and has been accepted for publication.

Accepted Manuscripts are published online shortly after acceptance, before technical editing, formatting and proof reading. Using this free service, authors can make their results available to the community, in citable form, before we publish the edited article. We will replace this *Accepted Manuscript* with the edited and formatted *Advance Article* as soon as it is available.

You can find more information about *Accepted Manuscripts* in the Information for Authors.

Please note that technical editing may introduce minor changes to the text and/or graphics, which may alter content. The journal's standard Terms & Conditions and the Ethical guidelines still apply. In no event shall the Royal Society of Chemistry be held responsible for any errors or omissions in this *Accepted Manuscript* or any consequences arising from the use of any information it contains.

ROYAL SOCIETY OF CHEMISTRY

www.rsc.org/faraday_d

CREATED USING THE RSC LaTeX PCCP ARTICLE TEMPLATE – SEE www.rsc.org/electronicfiles FOR DETAILS
PAPER www. rsc.org/faraday_d | Faraday Discussions

Faraday efficiency and mechanism of electrochemical surface reactions: CO_2 reduction and H_2 formation on Pt(111)

Javed Hussain,[a] Hannes Jónsson,[a,b] and Egill Skúlason*[a]

An atomic scale model of the electrical double layer is used to calculate the mechanism and rate of electrochemical reduction of CO_2 as well as H_2 formation at a Pt(111) electrode. The water layer contains solvated protons and the electrode has excess electrons at the surface. Density functional theory within the generalized gradient approximation is used to describe the electronic structure while the mechanism and activation energy of the various elementary reactions is obtained by calculating minimum energy paths using the nudged elastic band method. The applied electrical potential is deduced from the calculated work function. The optimal reaction mechanism for CO_2 reduction to either methane or methanol is found and the estimated rate compared with that of the competing reaction, H_2 formation. When the free energy of only the intermediates and reactants is taken into account, not the activation energy, Pt(111) would seem to be a good electrocatalyst for CO_2 reduction, significantly better than Cu(111). This, however, contradicts experimental findings. Detailed calculations reported here show that the activation energy for CO_2 reduction is high for both Heyrovsky and Tafel mechanisms on Pt(111) in the relevant range of applied potential. The rate-limiting step of the Heyrovsky mechanism, $*COOH + H^+ + e^- \rightarrow *CO + H_2O$, is estimated to have an activation energy of 0.95 eV at -0.9 V vs. standard hydrogen electrode. Under the same conditions, the activation energy for H_2 formation is estimated to be only 0.5 eV. This explains why attempts to reduce CO_2 using platinum electrodes have produced only H_2. A comparison is made with analogous results for Cu(111) [J. Hussain *et al.* Proc. Comp. Sci. 51, 1865 (2015)] where a reaction mechanism with low activation energy for CO_2 electroreduction to methane was identified. The difference between the two electrocatalysts is discussed.

1 Introduction

In the last couple of decades, computational methods based on density functional theory (DFT) for describing electronic degrees of freedom and rate theory, such as transition state theory (TST), for describing atomic degrees of freedom have been highly successful in describing chemical processes taking place at metal surfaces. The kinetics of surface catalyzed reactions have been described in great detail and the results found to be in close correspondence with experimental mea-

[a] *Science Institute and Faculty of Physical Sciences, University of Iceland VR-III, 107 Reykjavík, Iceland. Tel: +354 525 4684; E-mail: egillsk@hi.is*
[b] *Department of Applied Physics, Aalto University, Espoo, FI-00076, Finland.*

surements[1,2]. This has opened the possibility of designing new heterogeneous catalysts in a rational way based on computational predictions[3].

Analogous calculations of electrochemical reactions have been hampered by the complexity of the system. In addition to the solid surface and adsorbed species, it is necessary to describe the electrolyte, typically a liquid with solvated ions, as well as the effect of the electrical potential. Several theoretical approaches have been proposed, representing different levels of approximation and considerable advance has been made in recent years. A few reviews of theoretical approaches to electrochemical simulations have been published recently[4–9].

The charge at the surface of an electrode creates a cloud of counter charge in the electrolyte to form what is referred to as the electrical double layer. This has been analysed extensively using statistical mechanics[10,11]. The charge at the electrode surface is screened so the electrical field is limited to a narrow region near the electrode. As a result, the two electrodes can be treated separately as half cells. By convention the potential of a half cell is measured with respect to the standard hydrogen electrode (SHE). It is, however, more convenient in computer simulations to use the vacuum as a reference[12–16].

Two different levels of atomic scale simulations have mainly been used to study electrochemical systems. In the simpler one, the free energy of the various intermediates in an electrochemical reaction is first estimated in the absence of an electrolyte and of an applied electrical potential, but then the effect of the applied potential is estimated by adding $-eU$ for each pair of electron and proton added, where e is the charge of the electron and U is the applied potential[17]. An estimate of the onset potential is obtained as the applied potential for which none of of the elementary steps is uphill in free energy. We will refer to this as the thermochemical model (TCM).

In a more detailed model, the electrical double layer is simulated including solvated ions and excess electrons at the electrode and the transition paths for the elementary steps are calculated to estimate the activation energy and reaction rate as a function of electrical potential[14,18,19]. As will be demonstrated below, the more detailed simulation methodology is needed to identify the mechanism and calculate the rate of complex electrochemical reactions.

A particularly important electrochemical reaction which is actively studied today is the reduction of CO_2 to form hydrocarbons and alcohols[20]. Extensive, experimental work using pure transition metal electrodes has been carried out by Hori and coworkers[21–23]. When copper electrodes were used, a significant yield of hydrocarbons and alcohols (72%) such as CH_4, C_2H_4, C_2H_5OH, C_3H_7OH, C_2H_6, C_3H_5OH, CH_3CHO, and C_2H_5CHO was obtained. However, no other transition metal electrode was found to produce a significant yield of hydrocarbons or alcohols. A few example results from Hori's review article[23] are listed in Table 1. This work has inspired many research groups to investigate the CO_2 electroreduction reaction (CER) at copper electrodes. Recent experimental measurements have detected a significantly greater variety of products formed at copper electrodes[24] as well as electrodes of other pure metals such as Pt, Ni, Fe, Au, Ag, and Zn[25]. The rate (current density) of methane formation was found to be significantly higher on Cu electrodes than any of the other metals.

The detailed mechanism and factors controlling selectivity have also being studied. The surface morphology of polycrystalline copper has been shown to

Table 1 Experimentally measured Faradaic yield in CO_2 reduction using various transition metal electrodes, at 5 mA/cm^2 current density in a 0.1 M $KHCO_3$ buffer at 18.5 °C, as summarized by Hori[23]. The hydrocarbons and alcohols (HCAs) formed at copper electrodes are predominantly CH_4, C_2H_4, C_2H_5OH, C_3H_7OH, C_2H_6, C_3H_5OH, CH_3CHO, and C_2H_5CHO.

Electrode metals	Potential vs. SHE (eV)	Faradiac efficiency (%)			
		HC	CO	HCOOH	H_2
Au	-1.14	0.0	87.1	0.7	10.2
Ag	-1.37	0.0	81.5	0.8	12.4
Pd	-1.20	2.9	28.3	2.8	26.2
Cu	-1.44	72.3	1.3	9.4	20.5
Ni	-1.48	2.1	0.0	1.4	88.9
Pt	-1.07	0.0	0.0	0.1	95.7

affect the selectivity of products[26]. Electrodes consisting of a Cu overlayer on Pt have also been studied[27,28]. The CO_2 electroreduction involves a complicated network of reaction paths where several factors, including the morphology of the electrode surface, the pH of the electrolyte[29,30] and the electrode potential affect the mechanism and selectivity, for example whether C_1 or C_2 products are formed[31].

Significant progress has been made on the theoretical modeling of these processes. Since CO_2 is a closed shell molecule, one might expect that the binding of the molecule to the electrode surface would be limiting factor. DFT calculations including an applied electric field have, however, shown that with applied bias, CO_2 can bind chemically to an edge on a Pt(110)-(1x2) surface[32], and the same can likely occur at steps on the Pt(111) surface.

Peterson and co-workers estimated the onset potential for various products of CO_2 electroreduction using the TCM for a stepped Cu surface[33]. The results were in agreement with the measured onset potential for the various reduction products at Cu electrodes observed by Hori and co-wokers[23]. A step on the Cu(211) surface was shown to be slightly more reactive than a flat Cu(111) surface, with a lower onset potential by 0.1 V[34]. Peterson and Nørskov[35] and Shi *et al.*[36] used linear scaling relations for the adsorption energy of the various intermediates to create a 'volcano' graph showing how the rate-limiting step varies as a function of the binding energy of *CO over a range of transition metal surfaces. Cu indeed sits at the top of the volcano, i.e. has the lowest predicted overpotential for the stepped surfaces. The metals that bind CO less strongly, such as Au and Ag, reduce CO_2 only to CO because it desorbs from the surface before further reduction can occur. The metals that bind CO more strongly than Cu, such as Pt, should in principle also be able to reduce CO_2 to hydrocarbons or alcohols. The onset potential estimated from TCM is, in fact, only slightly higher, by 0.1 V, for a stepped Pt surface than a stepped Cu surface. Furthermore, the flat Pt(111) surface is predicted to have a much lower onset potential, of only -0.35 V[37]. The TCM, thereby, predicts Pt to be a much better electrocatalyst for CO_2 reduction than Cu, in clear contradiction with experiments.

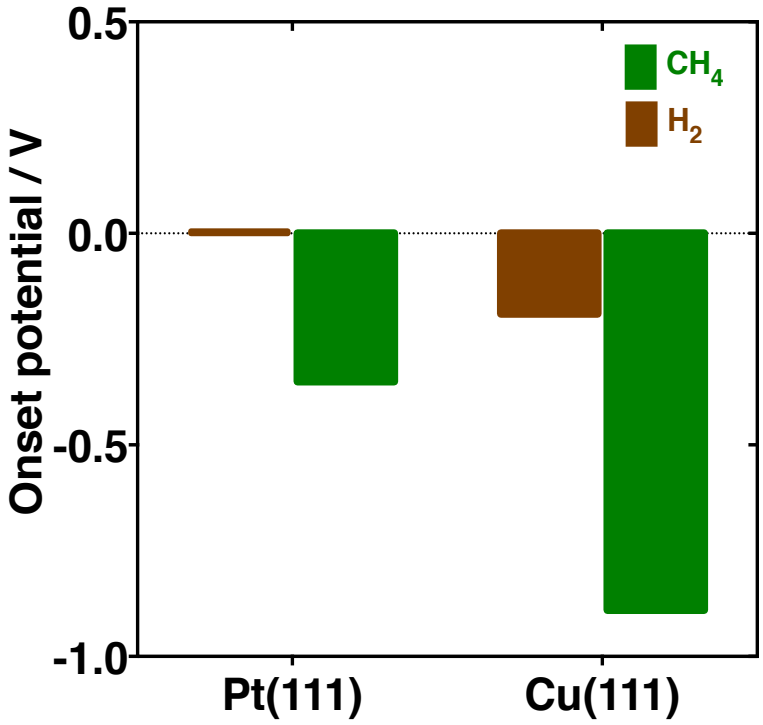

Fig. 1 Estimates of the onset potential for electrochemical CO_2 reduction to form CH_4 (from ref.[37]) and H_2 formation (from ref.[19]) on Pt(111) and Cu(111) surfaces obtained by using the thermochemical model, where only the free energy of intermediates and reactants is taken into account, not the activation energy. The overpotential for CO_2 reduction on Pt(111) is significantly lower than on Cu(111). Also, while the formation of H_2 is favored over CO_2 reduction on Pt(111) because it has a smaller overpotential, this difference in overpotentials is even larger for Cu(111). On both accounts, one would conclude that Pt is a better CO_2 electrocatalyst than Cu. But, the experimental evidence shows the opposite. Cu is the best CO_2 electrocatalyst known to date, while only H_2 is formed on Pt electrodes. Clearly, it is essential to take activation energy of the elementary steps into account when estimating the rate of these reactions.

The competing reaction, formation of H_2, also needs to be taken into account. The TCM has previously been used to estimate onset potential of this reaction[19]. The results of TCM calculations for both CO_2 electroreduction and H_2 formation (the so-called hydrogen evolution reaction, HER) on Pt(111) and Cu(111) are summarized in Fig. 1. One might conclude from the results on Pt(111) that CO_2 reduction does not occur because the overpotential is so much lower for H_2 formation. But, this is even more so the case for Cu(111) where the overpotential difference is even larger and yet CO_2 electroreduction is observed to take over H_2 formation in terms of Faradaic yield at a potential of around -0.9 V. The TCM model is, therefore, found to be unable to explain the comparison between Pt and Cu electrodes as electrocatalysts for CO_2 reduction.

The obvious limitation of the TCM is that it does not take activation energy

into account, i.e. the energy of transition states for the elementary processes. This requires more detailed modeling and is computationally more intensive than TCM calculations. Calculations of minimum energy paths for some of the critical elementary steps in CO_2 reduction on Pt(111) were carried out by Shi *et al.*[38]. They simulated the Heyrovsky mechanism for the reduction of CO_2 to form *COOH, *CO, *COH and then *C. A direct addition of a proton to the O-atom of the OH group and addition of an electron from the electrode, *COOH + H^+ + e^- $\rightarrow$ *CO + H_2O, was found to have an energy barrier of 0.5 eV, while the following step, *CO + H^+ + e^- $\rightarrow$*COH was found to have a lower energy barrier. The subsequent step, *COH + H^+ + e^- $\rightarrow$ *C + H_2O, was estimated to be the rate-limiting step with an activation energy of 0.55 eV. With a typical pre-exponential factor of 10^{12} sec^{-1}, a transition with an activation energy of 0.55 eV occurs on the time scale of a millisecond. Shi *et al.* concluded that the activation energy for the Heyrovsky mechanism of CO_2 electroreduction was low enough for the reaction to be active. The question, therefore, remained why Pt electrodes are found not to catalyze CO_2 electroreduction in experiments.

The calculations of Shi *et al.* were, however, done with a proton concentration corresponding to an applied voltage of around -2 V vs. SHE. This is a significantly larger negative potential than the one used in the experiments of Hori *et al.*, -1.07 V and of Kuhl *et al.*, -0.65 V to -0.9 V[23,25]. At a smaller negative potential the activation energy is expected to be higher[19]. Furthermore, at an applied potential of -2 V vs. SHE, protons are predicted to adsorb on the Pt(111) surface more strongly than CO, so the surface is expected to be covered with H-adatoms[14,19]. Similar considerations regarding the shift in the overlayer composition with bias have been discussed in the context of N_2 reduction[39–41].

Calculations of the activation energy for a given value of the applied potential are not straight forward because the number of dissolved protons in the dielectric and the number of excess electrons at the surface of the electrode changes as the reaction occurs. It is, therefore, important to carry out the simulation for several systems of different size and extrapolate to infinite size[18,19]. More approximate calculations of activation energy for CO_2 electroreduction on Cu surfaces have been carried out by Nie *et al.*, Cheng *et al.* and Xiao *et al.*[42–44] where the effect of the applied potential on the activation energy was estimated with a $-eU$ correction term analogous to the TCM model.

In the present study, calculations of the mechanism and activation energy of CO_2 electroreduction on a Pt(111) surface are carried out. Both the Tafel mechanism (involving reaction with an H-adatom) and the Heyrovsky mechanism (involving reaction of a proton from the water layer and electron from the electrode) are considered to find the optimal reaction path as a function of applied potential from -2 V to +0.7 V. Detailed comparison is made with the experimental measurements on CO_2 electroreduction and with the rate of H_2 formation.

The article is organized as follows: In the following section, the methodology used in the calculations is described. In section 3, the results of the free energy calculations of CO_2 electroreduction on Pt(111) are presented, and comparison made between high and low H-adatom coverage. Results of the calculations of minimum energy paths and activation energy extrapolated to infinite system for all elementary steps for CO_2 electroreduction to form methane and methanol are presented and compared with the competing reaction of H_2 formation. Finally, a

comparison with the Cu(111) electrode is made.

2 Methodology

The electronic structure calculations were carried out using DFT within the RPBE generalized gradient approximation[45]. The RPBE functional was specifically designed to give an accurate estimate of the chemisorption energy of adatoms and admolecules on a solid surface. Recently, functionals including van der Waals interaction, *e.g.* BEEF-vdW, have been developed to account also for the dispersion interaction[46]. Studt *et al.* compared the energetics of CO and CO_2 hydrogenation to methanol with the RPBE and BEEF-vdW functionals[47]. They found a difference of less than 0.07 eV in the free energy of intermediates and activation energy for reactions of chemisorbed species whereas the difference was as large as 0.4 eV for physisorbed species such as HCOOH. Since all the species in the reaction paths we study here are chemisorbed, the inclusion of van der Waals forces is not expected to be important in the present case. A plane wave basis set was used with a cutoff energy of 350 eV to expand the valence electron orbitals and PAW method used to represent core electrons[48]. In all cases, an irreducible Monkhorst Pack grid was used to reduce the number of k-points.

The electrode was represented by a slab of three atomic layers with periodically repeated (3x4) or (6x4) super cells and including (4x4x1) or (2x4x1) k-point sampling, respectively. Atoms in the bottom two layers of the slabs were held fixed but atoms in the top layer were allowed to move. The RPBE lattice constant of Pt of 4.02 Å was used and the slabs were separated by 10 to 12 Å of vacuum. The dipole correction was used in all cases to decouple the electrostatic interaction between the periodically repeated slabs. The VASP software was used[49].

The atomic structure of the various reactants and products was found by minimizing the energy until atomic forces had dropped below 0.03 eV/Å. In order to model the water-solid interface as a function of electrode potential, a bilayer of water molecules was added to the surface. It has been observed experimentally and theoretically that water forms an ice-like hexagonal bilayer structure on P(111)[50,51]. In this structure, the oxygen atom in every other water molecule is bonded to an underlying metal atom and the molecule lies in a plane parallel to the surface while the remaining water molecules either point one hydrogen atom towards (H-down) or away (H-up) from the surface. Schnur and Gross performed *ab initio* molecular dynamics calculations at room temperature on several metal surfaces and found a mixture of H-up and H-down orientations on *e.g.* Pt(111) where the latter was twice as abundant[52]. Haq *et al.* found experimentally and theoretically a few other possible orientations of the water network on Ru(0001) with a similar energy as the H-up and H-down structures[53]. The effect of an electrical field corresponding to negative applied voltage makes the H-down orientation more stable than the H-up orientation[54,55]. We have chosen the H-down orientation in our bilayer model. Since we determine the applied potential in each system from the work function as described below, the dipole moment of the water structure directly affects the estimated applied potential. However, since there is a linear correlation between the energetics and the applied potential, the choice of water model does not affect the overall conclusions[19]. In order to charge the

interface, additional H-atoms are inserted in the water bilayer to form a solvated proton and additional electron at the electrode. By changing the number of H-atoms added, the electrostatic potential of the double layer can be tuned and it was chosen here to range from -2 V to +0.7 V vs. SHE, in order to compare the results to the experimental conditions for Pt electrodes in the experiments by Hori *et al.* and by Kuhl *et al.* (from around -1 to around -0.5 V vs. SHE).

Calculations of the free energy of the various molecules adsorbed on the surface were carried out using the harmonic approximation and experimental estimates of the entropy of gas phase species. The effect of the applied potential on the free energy along the reaction path was calculated by adding $-eU$ to the free energy for each electron/proton pair added, where e is the charge of the electron and U is the applied potential. The onset potential for a reaction path to become active is, within the thermochemical model, the value of U needed to make all elementary steps such that the free energy is unchanged or decreases [17]. This, however, neglects the effect of free energy barriers due to transition states.

A more accurate indicator of reaction rates was obtained by evaluating the minimum energy path (MEP) for some of the most important elementary steps, using the climbing image nudged elastic band (CI-NEB) method [56–58]. The work function was calculated for the initial states and saddle points of each reaction step that involves direct addition of a proton from the water layer and an electron from the electrode, i.e. a Heyrovsky mechanism. An extrapolation scheme was then used to estimate the activation energy at a fixed electric potential [8,18,19]. The problem here is that within the model used for the electrochemical double layer, the effective potential changes during a proton-electron transfer reaction, since there is a change in the number of hydronium ions in the water layer and excess electrons at the electrode surface. Thereby, the electrical potential changes during the reaction. This can affect the energetics considerably, most severely for small simulation cells [8,19]. The electrical potential should remain constant during the electrochemical reaction. By calculating the energetics in cells of varying size but with same initial potential and evaluating the energy of interest as a function of the change in the potential, an extrapolation to a zero change and infinite system limit is effectively obtained. This methodology for modeling the electrochemical solid-liquid interface has recently been reviewed [7–9].

The highest energy along the MEP gives the activation energy, E_a, within the harmonic transition state theory approximation, and the rate constant can be expressed as

$$k = \nu e^{-E_a/k_B T}. \quad (1)$$

The pre-exponential factor, ν, was taken to have a typical value of 10^{12} s^{-1} per reactive site on the surface. The surface area (in units of cm^2) per site, A/N, on Cu(111) and Pt(111) is: 6.13×10^{-16} and 6.64×10^{-16}, respectively. The current density is evaluated as $i = k$eN/A, where e is the electron charge [14,19]. The Faraday efficiency (current efficiency) is the current density divided by the total current density.

3 Results

The calculated free energy of intermediates along possible reaction paths for CO_2 reduction on Pt(111) are presented first. Thereafter, estimates are presented of

the energy barriers obtained from calculations of minimum energy paths for both Heyrovsky and Tafel mechanisms of all elementary steps in order to identify the rate-limiting step.

3.1 Free energy of intermediates on Pt(111)

The estimated free energy of intermediates indicates several likely paths for the reduction of CO_2 to form either methane or methanol, see Fig. 2(a) for a clean Pt(111) surface and Fig. 2(b) for a H-covered surface. The path with the lowest free energy rise involves formation of *CHOH. Two steps in the reaction path have nearly equal increase in free energy, of about 0.35 eV, on the clean surface (ca. 0.5 eV on the H-covered surface). These are first *CO $\rightarrow$ *COH and then *COH $\rightarrow$ *CHOH. From there, either *CH forms and then methane, or *CH_2OH forms and then methanol, or *CH_2 is formed and then methane. A slightly higher rise in free energy occurs by forming *C + H_2O instead of *CHOH, a path that is shown to lead to methane formation. Formation of *CHO instead of *COH involves a significantly higher rise in free energy in an elementary step, as has been noted previously[38,59] and is therefore deemed unlikely on Pt(111). The path involving formation of *C+H_2O was already calculated previously by Shi *et al.*[38] whereas the possibility of the *CHOH was not considered to our knowledge. The reduction of CO_2 to *COOH has the largest increase in free energy when the surface is covered with H adatoms, see Fig. 2(b).

3.2 Onset potential for reduction

The application of an external electrical potential, U, affects the free energy of the intermediates of the reduction path in such a way that a contribution of $\Delta G = -eU$ gets added whenever a H^+ and e^- react to add an H-atom to the ad-molecule. A calculated rise in the free energy at an elementary step of 0.35 eV can therefore be eliminated by applying an electrical potential of -0.35 V. In the TCM approximation it is assumed that a reaction path becomes active when no elementary step involves an increase in the free energy, so the onset potential can be estimated from the largest free energy increase in an elementary step in the reaction path[17]. The most endothermic elementary step then gives the estimate of the onset potential.

Applying this approximation to the free energy curves for CO_2 reduction on the clean Pt(111) surface and on the H covered Pt(111) surface, shown in Fig. 2, gives an estimate of the onset potential as -0.35 V for the former and -0.8 V for the latter. From these results, one would conclude that Pt(111) is one of the best electrocatalyst since the overpotential there is low. This is in contrast with the experimental observation that no significant reduction products from CO_2 are observed in experiments with platinum electrodes, even with applied potential of -1.07 V[23,25]. Clearly, some other factor than the free energy of intermediates affects the viability of the reduction reaction.

3.3 Activation energy

An important factor that is missing in the TCM is the activation energy of the elementary steps. While the success of the TCM indicates that it is often a good

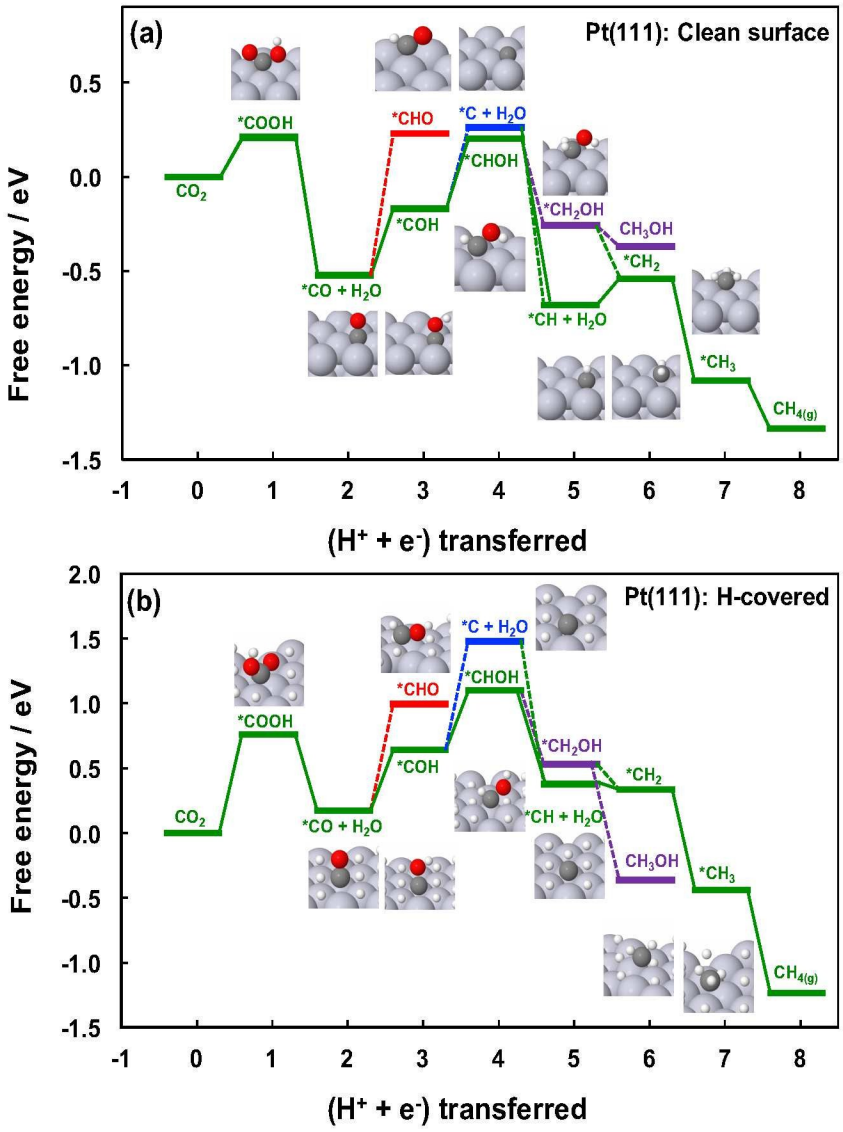

Fig. 2 Calculated free energy of various intermediates of CO_2 reduction to methane and methanol by the thermochemical model (water layer not present and activation energy not included), (a) on a clean Pt(111) surface, (b) on a H covered Pt(111) surface. Contributions to the free energy at 300 K (zero point energy (ZPE) correction, enthalpic temperature correction, and vibrational entropy (-TS) correction) of the various reaction intermediates were taken from tables in the supporting information with ref.[33] (Tables S3 and S5) and[60] (Table S2) where the adsorbed species were calculated on a Cu(211) surface. According to the TCM, the formation of *COOH, *COH and either *CHOH or *C are likely the potential limiting steps on Pt(111), the rise in free energy indicating an onset potential of -0.35 V on the clean surface while an onset potential of -0.8 V on the H covered surface.

approximation, this appears not be the case for the electroreduction of CO_2. In order to go beyond the TCM, we have calculated minimum energy paths (MEPs) for the two elementary steps that involve a large rise in free energy (as seen in Fig. 2), the *COH → *CHOH step and the *COH → *C + H_2O step. The MEPs are shown in Fig. 3. The MEPs were calculated for both a Heyrovsky mechanism where a proton from the water solution attaches directly onto the admolecule and an electron simultaneously is added from the electrode as well as a Tafel mechanism where a H-adatom reacts with the admolecule. The proton concentration

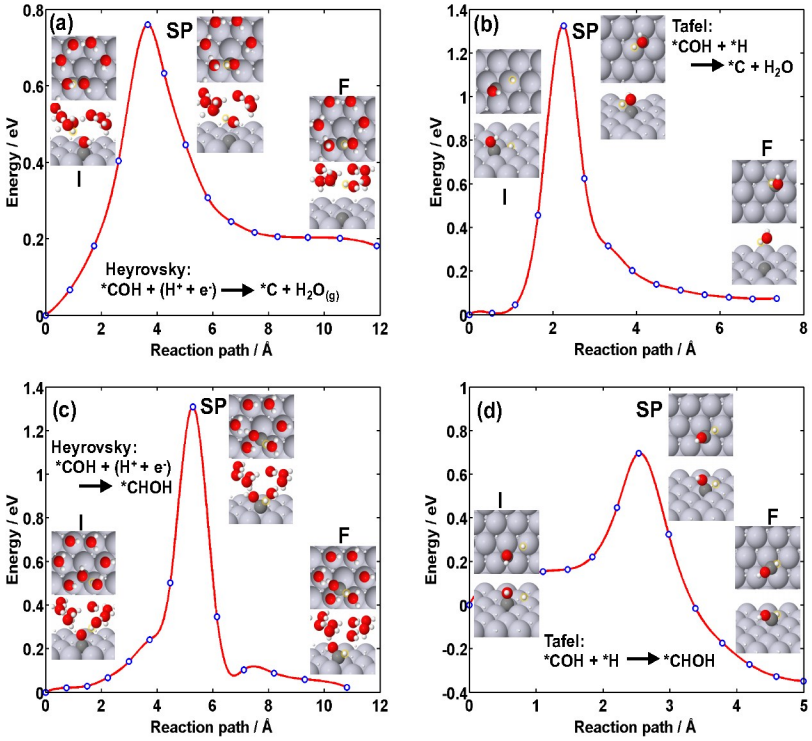

Fig. 3 Minimum energy paths for two elementary steps in the reduction of CO_2 on Pt(111). *COH is reduced to either *C (a and b) or *CHOH (c and d) by Heyrovsky mechanism where H^+ from the solution and e^- from the electrode are added (a and c) or Tafel mechanisms where an H-adatom is added (b and d). The calculations of the Heyrovsky mechanism uses a slab containing (3x4) surface unit cells and includes 8 water molecules in a bilayer structure in (c) where one H_2O molecule is removed to make room for the H_2O molecule that is formed during the reaction in (a). The calculations for the Tafel mechanism uses (3x4) surface unit cells. In the calculations of the Heyrovsky mechanism, one H-atom is added to the water bilayer to form a proton/electron pair, which reacts during the transition. The calculations show that the Heyrovsky mechanism is preferred for the formation of *C, while the Tafel mechanism is preferred for the formation of *CHOH. In either case, the activation energy is large, providing an explanation of why CO_2 electroreduction is not observed experimentally when platinum electrodes are used.

and excess electrons at the electrode surface are consistent here with an applied

voltage of around -0.9 V, similar to conditions in the experiments of Hori and co-workers and Kuhl and co-workers. The surface is expected to have high coverage of H-adatoms under these conditions, essentially a full monolayer[19]. The H-adatoms occupy FCC sites, while the *COH admolecule sits at an on-top site. In simulations of the Heyrovsky mechanism, a double layer is set up by including a water bilayer and H-atoms are then added to the water layer to form solvated hydronium ions and excess electrons at the electrode. Analogous calculations have previously been performed for H_2 formation[14,19]. One water molecule has been removed from the bilayer to make room for the H_2O molecule that is formed during the *COH $\rightarrow$ *C + H_2O reaction. The *COH forms hydrogen bonds to two neighboring water molecules, similar as in the simulations by Shi *et al.*[38]. The calculations carried out for the Tafel mechanism did not include a water bilayer since a solvated proton is not directly involved in the reaction. Simulations of H_2 formation where this approximation was tested have shown that accurate estimate of the activation energy can be obtained without the water layer for a Tafel mechanism[14]. But, the calculated energy difference between the saddle point configuration and the initial state needs to be corrected for the change in the number of hydrogen bonds for some of the elementary steps in the CO_2 electroreduction.

The results of the calculations are shown in Fig. 3. The calculated activation energy for both elementary steps and both reaction mechanisms is high, around 0.7 eV or larger. The lowest activation energy is found for the Tafel mechanism for the *COH$\rightarrow$*CHOH step. This, however, is a high barrier for a reaction at room temperature and would lead to an insignificant rate. Given that DFT calculations tend to underestimate the energy of transition states with respect to stable states (because of self-interaction error[61,62]), this result indicates that low reduction activity at platinum electrodes can be traced to large energy barriers for the reduction of *COH.

Similar calculations for the Heyrovsky mechanism of the *COH $\rightarrow$ *C + H_2O step have been reported by Shi *et al.*[38] but their simulation was different in two respects. First, the surface did not have high coverage of H-adatoms and, secondly, the concentration of protons/electrons in the double layer corresponded to an applied voltage of ca. -2 V. The value of the activation energy reported by Shi *et al.* was therefore lower, 0.55 eV, compared with the value of 0.74 eV obtained here at an applied potential of -0.9 V. A larger, negative applied potential is expected to result in a lower activation energy.

The effect of changes in hydrogen bonding on the activation energy of Tafel reaction steps is estimated by counting the number of bonds in the initial state and final state and assuming an intermediate hydrogen bond energy at the transition state. For the *COH + *H $\rightarrow$ *C + H_2O step, shown in Fig. 3(b), the initial state, *COH, can donate one H-bond and accept two H-bonds while the final state, *C + H_2O, can donate two H-bonds and accept two H-bonds. The final state will thus be stabilized by one more H-bond than the initial state, around 0.25 eV[63,64]. This could result in a decrease of the activation energy of about 0.1 to 0.2 eV, assuming a BEP relation[65]. Since the activation energy obtained from the MEP without water is high, around 1.3 eV, this reaction mechanism is in any case not likely to be active at room temperature. The effect of H-bonds will not change that conclusion. The Heyrovsky mechanism for the formation of *C +

H_2O, shown in Fig. 3(a) will be considerably faster than the Tafel mechanism.

The calculated activation energy for the Tavel mechanism for *CHOH formation is slightly lower (0.69 eV in Fig. 3(d)) than for the Heyrovsky mechanism for *C + H_2O formation (0.74 eV in Fig. 3(a)). A correction because of hydrogen bonding is not needed here for the Tafel mechanism for *CHOH formation. This intermediate on the Pt(111) surface has not been considered as a key intermediate in previous DFT calculations to our knowledge. The Heyrovsky mechanism for the formation of *CHOH has higher activation energy, 1.3 eV, see Fig. 3(c). This is understandable from the fact that the solvated proton has to travel long distance to reach the C-atom of the *COH admolecule. It is easier for a nearby H-adatom to attach to the C-atom (Fig. 3(d)). The H-bonding network is not likely to affect the energetics here since the number of H-bonds in the initial and final states are expected to be the same. Further reduction of *CHOH can give either methane or methanol.

3.4 Extrapolation to constant potential

The calculations of the minimum energy paths and the activation energy of steps involving the Heyrovsky mechanism are problematic in that the effective electric potential due to the double layer changes when a proton reacts and is removed from the layer. The larger the system is and the larger the number of protons, the smaller the effect is. By carrying out the calculations for two systems with different size but same concentration of protons, and thereby corresponding to the same potential, an extrapolation can be made to the infinite size limit where the removal of a proton does not change the potential[8,18,19]. This has been done for the *COH + H^+ + e^- →*C + H_2O step, the *COH + H^+ + e^- →*CHOH step and the H^+ + e^- →*H step when extrapolating to a proton-electron concentration per surface Pt atom of 1/12 (which corresponds to applied potential of -0.9 V[66]) and for the CO_2 + H^+ + e^- →*COOH step and the *COOH + H^+ + e^- →*CO + H_2O step when extrapolating to a proton-electron concentration per surface Pt atom of zero (which corresponds to applied potential of +0.7 V[66]). The results are shown in Fig. 4. The calculated activation energy for all the elementary steps is shown as a function of the change in potential from the initial state to the saddle point, ΔU, during the reaction. For the systems considered here at -0.9 V, the calculated activation energy for the reduction steps of CO_2 electroreduction does not change significantly when extrapolating to ΔU = 0 V. This means that the results of the NEB calculations shown in Fig. 3 already give a good estimate of the activation energy when considering reduction processes at negative potentials. This has been seen before for other reduction processes when the applied potential is negative enough[8,19]. When the proton is transferred all the way to the surface via the Volmer reaction at this same potential, -0.9 eV, the activation energy changes slightly more as the supercell is increased and the extrapolation scheme is then needed. On the other hand, for the reduction processes at +0.7 V, the activation energy does change significantly, as seen in Fig. 4, when extrapolating to infinite systems which is consistent with previous results[8,19].

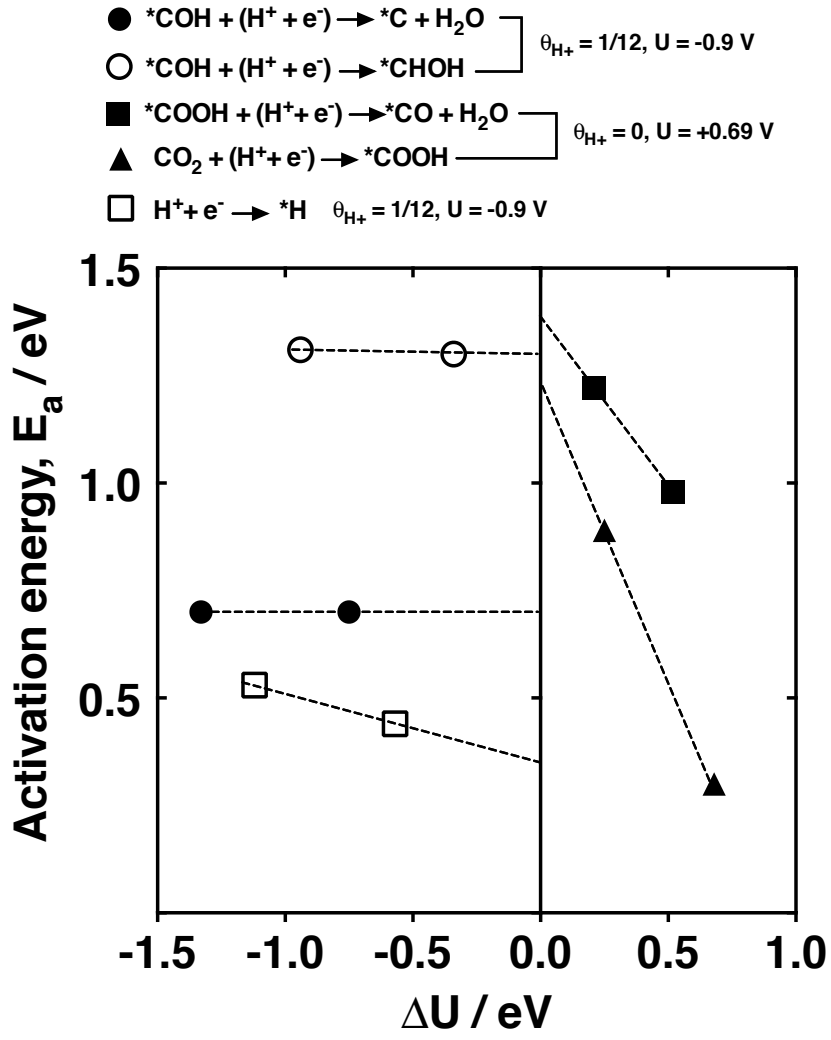

Fig. 4 Extrapolation of calculated activation energy of the Volmer reaction ($H^+ + e^- \rightarrow$*H) and the Heyrovsky reaction for four different elementary steps of CO_2 electroreduction on Pt(111) to conditions where the change in the corresponding electrical potential, ΔU, is zero, from the initial state to the saddle point. The data points are obtained from calculations on slabs including (3x4) and (6x4) surface unit cells, with 1 and 2 additional H-atoms added, respectively, to the water bilayer to create proton-electron pairs. The change in the electrical potential is deduced from calculated values of the work function. Extrapolations are made for a proton/Pt surface atom ratio of θ_{H^+} = 1/12 as well as 0.

3.5 Mechanism for methane and methanol formation

The free energy change and activation energy for each elementary step in CO_2 electroreduction to either methane or methanol at -0.9 V potential on a Pt(111)

electrode are shown in Fig. 5. The activation energy was calculated for both a Heyrovsky-type and a Tafel-type reaction mechanism and the lower value is shown. The rate-limiting step turns out to be the *COOH + H^+ + e^- →*CO + H_2O reaction with a 0.95 eV barrier at -0.9 V via a Heyrovsky mechanism. All other steps have activation energy lower than 0.76 eV at this potential. It is surprising to find this to be the rate-limiting step since it involves a significant drop in free energy (see Fig. 2). This shows clearly how important it is to calculate the activation energy for all the elementary steps. After the rate-limiting step, when *CO has been formed on the surface, *COH is more likely to form than *CHO, both according to the thermodynamics as well as the kinetics. The subsequent step either involves *CHOH formation via a Tafel mechanism or *C + H_2O formation via a Heyrovsky mechanism. The activation energy for the two is quite similar, 0.69 eV and 0.74 eV, respectively. Since different reaction mechanisms and therefore atomic models are used here we do not conclude which species will be more dominant on the surface, the *CHOH or the *C species. Further reduction of either of these two species can result in *CH forming, and then finally methane formation. The *CHOH species may be reduced to either *CH + H_2O or to *CH_2OH. The activation energy for these two steps is almost the same, 0.74 eV and 0.76 eV, respectively. Both *CH and *CH_2OH could be present on the surface. The *CH_2OH species will then be reduced to methanol with a low barrier of 0.38 eV via a Heyrovsky mechanism rather than formation of *CH_2 + H_2O which has an activation energy of 0.88 eV in a Heyrovsky mechanism. However, the *CH species can be reduced to *CH_2 with a 0.69 eV barrier. The final step to form methane involves a Heyrovsky reaction where a proton is added to the *CH_3 species, with an activation energy of 0.76 eV.

Clearly, the electroreduction of CO_2 involves a complex reaction network. The rate limiting step for methane and methanol formation turns out to be the same, i.e. the formation of *CO with a barrier of 0.95 eV at a potential of -0.9 V. This is in good agreement with the experiments on Pt at this potential where the rate of methane and methanol formation was found to be similar[25]. After the rate limiting step, the highest activation energy towards methanol is in *CH_2OH formation, while the highest activation energy towards methane is the reduction of *CH_3. In both cases the activation energy is 0.76 eV at a potential of -0.9 V.

3.6 Potential dependent activation energy

The activation energy of the rate-limiting step, *COOH + H^+ + e^- →*CO + H_2O, was calculated for an applied potential of -0.9 V on Pt(111) as shown in Fig. 5. The variation of the activation energy as a function of the applied potential, from -2 V to +0.7 V has also been calculated and is shown in Fig. 6. The potential dependence of the activation energy is strong, it varies from around 0.45 eV to around 1.3 eV over this range in applied potential. The calculations are in close agreement with the calculations by Shi *et al.*[38] where an activation energy of 0.5 eV at an applied potentials of around -2 V was obtained. The only difference between their calculation and ours is the H-adatom coverage on the surface. In our calculations a full monolayer of H adatoms is present on the surface whereas the calculations by Shi *et al.* did not include any H adatoms. The strong dependence of the activation energy on the applied potential shows that

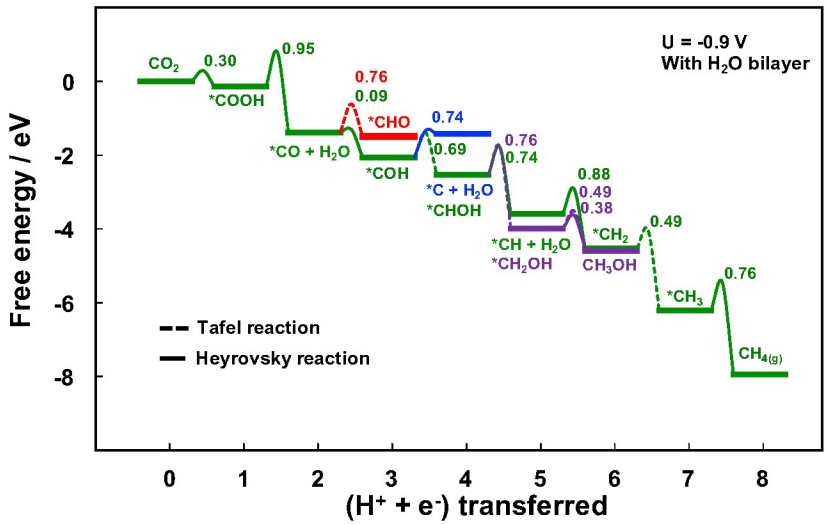

Fig. 5 Calculated free energy change and activation energy (given by numbers next to barriers in units of eV) in electroreduction of CO_2 to both methane and methanol at a Pt(111) surface when the applied potential is -0.9 V. The optimal mechanism to form methane is shown (green), as well as several alternative mechanisms involving different intermediates: *CHO instead of *COH (red), *C instead of *CHOH (blue), *CH_2OH instead of *CH (purple). Reduction of *CH_2OH then leads to formation of methanol (purple). Both Heyrovsky (full line) and Tafel (dashed line) mechanisms are considered.

while the activation energy is low at -2 V, it is high at a potential of -0.65 V to -1.1 V used in the experiments[23,25]. Our calculations, thereby, explain why the rate of methane and methanol formation is as low on Pt electrodes as has been observed experimentally. The estimated rate of CO_2 electroreduction using the calculated activation energy and assuming a pre-exponential factor of 10^{12} per site per second is used to calculate current density for detailed comparison with experimental data[25,66], as shown in Fig. 6(b). Results of similar calculations for H_2 formation are also shown. The agreement with experiment is remarkably good considering that no parameter is adjusted in the calculation to fit the experimental data. The calculations explain why low current efficiency is obtained for CO_2 electroreduction and high current efficiency is obtained for H_2 formation (Fig. 6(c)). In Fig 6(d,e,f), similar calculations are shown for Cu(111) and a comparison with experimental results for a copper electrode[24,25,66]. Again, the agreement is excellent. The cross-over in the rate of H_2 formation and CO_2 electroreduction at -0.9 V is explained by the changes in activation energy of the rate-limiting steps. The Faraday efficiency of CO_2 electroreduction becomes higher than for H_2 formation on copper when the applied potential is more negative than -0.9 V.

4 Conclusions

The goal of this study was to gain better understanding of why attempts to electrochemically reduce CO_2 on Pt electrodes have not proved to be successful,

while a significant yield of hydrocarbons and alcohols has been obtained with Cu electrodes. Simulations of the electrical double layer and calculations of reaction paths for the various elementary steps where carried out and for conditions corresponding to the ones in the experiments of Hori and coworkers [21–23] and Kuhl and coworkers [24,25]. The optimal reaction mechanism for both methane and methanol formation was identified. A relatively large activation energy was obtained for several of the elementary steps, and a strong potential dependence found. Close agreement with the measured current density and Faradaic yield was obtained for both methane and methanol formation and the fact that mostly H_2 is formed. The calculations presented here show that the low rate of methane and methanol formation at Pt electrodes is due to large activation energy in CO_2 electroreduction.

5 Acknowledgements

This work was supported by the Icelandic Research Fund, Nordic Energy Research through the NISFD network, the University of Iceland Doctoral Scholarship Fund and the Academy of Finland FiDiPro program (grant 263294). The

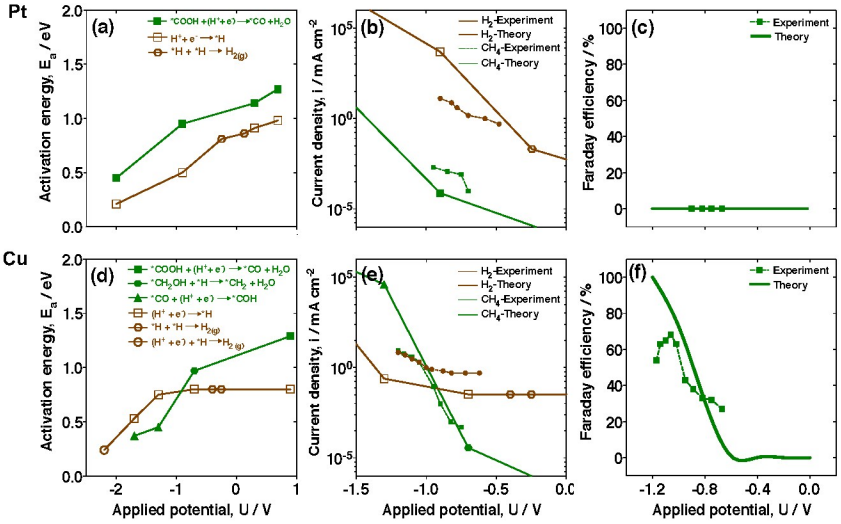

Fig. 6 Calculated activation energy of the rate-limiting step shown in Fig. 5 of CO_2 electroreduction and H_2 formation at (a) Pt(111) and (d) Cu(111) surfaces as a function of applied potential. The current density is calculated from an Arrhenius expression for the rate using the calculated activation energy and assuming a pre-exponential factor of 10^{12} per site per second at (b) Pt(111) and (e) Cu(111). Faraday efficiency (current efficiency) in CO_2 reduction as a function of applied potential for (c) Pt(111) and (f) Cu(111) electrodes. The agreement with experiments [24,25] is remarkably good considering that no parameter is adjusted in the calculation to fit the experimental data. These calculations show that the low rate and low efficiency of methane formation at Pt electrodes is due to large activation energy in CO_2 electroreduction and low activation energy in H_2 formation. For Cu(111), a cross-over in activation energy occurs for these two processes, consistent with the experimentally observed trends on Cu electrodes.

calculations were carried out using the Nordic High Performance Computing (NHPC) facility in Iceland.

References

1 K. Honkala, A. Hellman, I. N. Remediakis, A. Logadóttir, A. Carlsson, S. Dahl, C. H. Christensen and J. K. Nørskov, *Science*, 2005, **307**, 555–8.

2 J. K. Nørskov, F. Abild-Pedersen, F. Studt and T. Bligaard, *Proc. Natl. Acad. Sci. USA.*, 2011, **108**, 937–43.

3 J. K. Nørskov, T. Bligaard, J. Rossmeisl and C. H. Christensen, *Nat. Chem.*, 2009, **1**, 37–46.

4 J. Rossmeisl, J. Greeley and G. S. Karlberg, *Electrocatalysis and Catalyst Screening from Density Functional Theory Calculations in Fuel Cell Catalysis: A Surface Science Approach*, (ed M. T. M. Koper), John Wiley & Sons, Inc., Hoboken, NJ, USA., 2009, pp. 57–92.

5 A. Gross and S. Schnur, in *Computational Chemistry Applied to Reactions in Electrocatalysis, in Catalysis in Electrochemistry: From Fundamentals to Strategies for Fuel Cell Development*, (eds E. Santos and W. Schmickler), John Wiley & Sons, Inc., Hoboken, NJ, USA., 2011, pp. 165–196.

6 Y. Zheng, Y. Jiao, M. Jaroniec and S. Z. Qiao, *Angew. Chem. Int. Ed.*, 2015, **54**, 52–65.

7 M. Nielsen, M. E. Björketun, M. H. Hansen and J. Rossmeisl, *Surf. Sci.*, 2014, **631**, 2–7.

8 E. Skúlason, *Procedia Comp. Sci.*, 2015, **51**, 1887–1896.

9 E. Skúlason and H. Jónsson, *Advances in Physics X, accepted for publication*, 2016, **1**,.

10 D. C. Grahame, *Chem. Rev.*, 1947, 441–501.

11 J. O. Bockris, M. A. V. Devanathan and K. Muller, *Proc. Roy. Soc, Ser. A.*, 1963, **274**, 55–79.

12 S. Trasatti, *Electrochim. Acta.*, 1991, **36**, 1659–1667.

13 C. D. Taylor, S. A. Wasileski, J.-S. Filhol and M. Neurock, *Phys. Rev. B.*, 2006, **73**, 165402–165416.

14 E. Skúlason, G. S. Karlberg, J. Rossmeisl, T. Bligaard, J. Greeley, H. Jónsson and J. K. Nørskov, *Phys. Chem. Chem. Phys.*, 2007, **9**, 3241–3250.

15 V. Tripkovic, M. Björketun, E. Skúlason and J. Rossmeisl, *Phys. Rev. B.*, 2011, **84**, 1–11.

16 T. Matsui, Y. Kitagawa, M. Okumura, Y. Shigeta and S. Sakaki, *J. Comput. Chem.*, 2013, **34**, 21–26.

17 J. K. Nørskov, J. Rossmeisl, A. Logadóttir, L. Lindqvist, J. R. Kitchin, T. Bligaard and H. Jónsson, *J. Phys. Chem. B.*, 2004, **108**, 17886–17892.

18 J. Rossmeisl, E. Skúlason, M. E. Björketun, V. Tripkovic and J. K. Nørskov, *Chem. Phys. Lett.*, 2008, **466**, 68–71.

19 E. Skúlason, V. Tripkovic, M. E. Bjørketun, S. Gudmundsdóttir, G. Karlberg, J. Rossmeisl, T. Bligaard, H. Jónsson and J. K. Nørskov, *J. Phys. Chem. C.*, 2010, **114**, 18182–18197.

20 D. T. Whipple and P. J. Kenis, *J. Phys. Chem. Lett.*, 2010, **1**, 3451–3458.

21 Y. Hori, A. Murata and R. Takahashi, *J. Chem. Soc. Faraday Trans. 1.*, 1989, **85**, 2309–2326.

22 Y. Hori, H. Wakebe, T. Tsukamoto and O. Koga, *Electrochim. Acta.*, 1994, **39**, 1833–1839.

23 Y. Hori, *Modern aspects of electrochemistry*, C.G. Vayenas, R.E. White, M.E. Gamboa- Aldeco, Eds.; (Springer, New York)., 2008, vol. 42, pp. 89–189.

24 K. P. Kuhl, E. R. Cave, D. N. Abram and T. F. Jaramillo, *Energy & Environ. Sci.*, 2012, **5**, 7050–7059.

25 K. P. Kuhl, T. Hatsukade, E. R. Cave, D. N. Abram, J. Kibsgaard and T. F. Jaramillo, *J. Am. Chem. Soc.*, 2014, **136**, 14107–14113.

26 W. Tang, A. A. Peterson, A. S. Varela, Z. P. Jovanov, L. Bech, W. J. Durand, S. Dahl, J. K. Nørskov and I. Chorkendorff, *Phys. Chem. Chem. Phys.*, 2012, **14**, 76–81.

27 R. Reske, M. Duca, M. Oezaslan, K. J. P. Schouten, M. T. M. Koper and P. Strasser, *J. Phys. Chem. Lett.*, 2013, **4**, 2410–2413.

28 A. S. Varela, C. Schlaup, Z. P. Jovanov, P. Malacrida, S. Horch, I. E. Stephens and I. Chorkendorff, *J. Phys. Chem. C.*, 2013, **117**, 20500–20508.

29 R. Kortlever, K. Tan, Y. Kwon and M. T. M. Koper, *J. Solid State Electrochem.*, 2013, **17**, 1843–1849.

30 K. J. P. Schouten, E. P. Gallent and M. T. M. Koper, *J. Electroanal. Chem.*, 2014, **716**, 53–57.

31 K. J. P. Schouten, Y. Kwon, C. Van der Ham, Z. Qin and M. T. M. Koper, *Chem. Sci.*, 2011, **2**, 1902–1909.

32 S. Gudmundsdóttir, W. Tang, G. Henkelman, H. Jónsson and E. Skúlason, *J. Chem. Phys.*, 2012, **137**, 164705.

33 A. A. Peterson, F. Abild-Pedersen, F. Studt, J. Rossmeisl and J. K. Nørskov, *Energy & Environ. Sci.*, 2010, **3**, 1311–1315.

34 W. J. Durand, A. A. Peterson, F. Studt, F. Abild-Pedersen and J. K. Nørskov, *Surf. Sci.*, 2011, **605**, 1354–1359.

35 A. A. Peterson and J. K. Nørskov, *J. Phys. Chem. Lett.*, 2012, **3**, 251–258.

36 C. Shi, H. A. Hansen, A. C. Lausche and J. K. Nørskov, *Phys. Chem. Chem. Phys.*, 2014, **16**, 4720–4727.

37 J. Hussain, E. Skúlason and H. Jónsson, *Procedia Comp. Sci.*, 2015, **51**, 1865–1871.

38 C. Shi, C. P. O'Grady, A. A. Peterson, H. A. Hansen and J. K. Nørskov, *Phys. Chem. Chem. Phys.*, 2013, **15**, 7114–7122.

39 E. Skúlason, T. Bligaard, S. Gudmundsdóttir, F. Studt, J. Rossmeisl, F. Abild-Pedersen, T. Vegge, H. Jónsson and J. K. Nørskov, *Phys. Chem. Chem. Phys.*, 2012, **14**, 1235–1245.

40 Y. Abghoui, A. L. Garden, V. F. Hlynsson, S. Björgvinsdóttir, H. Ólafsdóttir and E. Skúlason, *Phys. Chem. Chem. Phys.*, 2015, **17**, 4909–4918.

41 Y. Abghoui, A. L. Garden, J. G. Howalt, T. Vegge and E. Skúlason, *ACS Catal.*, 2016, **6**, 635–646.

42 X. Nie, M. R. Esopi, M. J. Janik and A. Asthagiri, *Angew. Chem. Int. Ed.*, 2013, **52**, 2459–2462.

43 T. Cheng, H. Xiao and W. A. Goddard, *J. Phys. Chem. Lett.*, 2015, **6**, 4767–4773.

44 H. Xiao, T. Cheng, W. A. Goddard and R. Sundararaman, *J. Am. Chem. Soc.*, 2016, **138**, 483–486.

45 B. Hammer, L. B. Hansen and J. K. Nørskov, *Phys. Rev. B.*, 1999, **59**, 7413–7421.

46 J. Wellendorff, K. T. Lundgaard, A. Møgelhøj, V. Petzold, D. D. Landis, J. K. Nørskov, T. Bligaard and K. W. Jacobsen, *Phys. Rev. B*, 2012, **85**, 235149.

47 F. Studt, F. Abild-Pedersen, J. B. Varley and J. K. Nørskov, *Catal. Lett.*, 2012, **143**, 71–73.

48 P. E. Blöchl, *Phys. Rev. B.*, 1994, **50**, 17953–17979.

49 G. Kresse and J. Hafner, *Phys. Rev. B.*, 1993, **47**, 558–561.

50 H. Ogasawara, B. Brena, D. Nordlund, M. Nyberg, A. Pelmenschikov, L. G. M. Pettersson and A. Nilsson, *Phys. Rev. Lett.*, 2002, **89**, 276102.

51 S. Meng, L. F. Xu, E. G. Wang and S. Gao, *Phys. Rev. Lett.*, 2002, **89**, 176104.

52 S. Schnur and A. Groß, *New Journal of Physics*, 2009, **11**, 125003.

53 S. Haq, C. Clay, G. R. Darling, G. Zimbitas and A. Hodgson, *Phys. Rev. B*, 2006, **73**, 115414.

54 A. Roudgar and A. Groß, *Chem. Phys. Lett.*, 2005, **409**, 157–162.

55 J. Rossmeisl, J. K. Nørskov, C. D. Taylor, M. J. Janik and M. Neurock, *Phys. Chem. B*, 2006, **110**, 21833–9.

56 H. Jónsson, G. Mills and K. W. Jacobsen, *Classical and Quantum Dynamics in Condensed Phase Simulations*, B. J. Berne, G. Ciccotti, and D. F. Coker, Eds. (World Scientific, Singapore), 1998, p. 385.

57 G. Henkelman, B. P. Uberuaga and H. Jónsson, *J. Chem. Phys.*, 2000, **113**, 9901–9904.

58 G. Henkelman and H. Jónsson, *J. Chem. Phys.*, 2000, **113**, 9978–9985.

59 L. Árnadóttir, E. M. Stuve and H. Jónsson, *Chem. Phys. Lett.*, 2012, **541**, 32–38.

60 P. Hirunsit, *J. Phys. Chem. C*, 2013, **117**, 8262–8268.

61 S. Klüpfel, P. Klüpfel and H. Jónsson, *J. Chem. Phys.*, 2012, **137**, 124102.

62 H. Jónsson, *Proc. Natl. Acad. Sci.*, 2011, **108**, 944–949.

63 J. W. Larson and T. B. McMahon, *Inorg. Chem.*, 1984, **23**, 2029–2033.

64 G. S. Karlberg and G. Wahnström, *Phys. Rev. Lett.*, 2004, **92**, 136103–136107.

65 S. Wang, V. Petzold, V. Tripkovic, J. Kleis, J. G. Howalt, E. Skúlason, E. M. Fernandez, B. Hvolbaek, G. Jones, A. Toftelund, H. Falsig, M. Björketun, F. Studt, F. Abild-Pedersen, J. Rossmeisl, J. K. Nørskov and T. Bligaard, *Phys. Chem. Chem. Phys.*, 2011, **13**, 20760–20765.

66 J. Hussain, H. Jónsson and E. Skúlason, *Submitted.*, 2016.